The Topology of Skeletons and Offsets

Stefan Huber[1]

1 **B&R Industrial Automation**
`stefan.huber@br-automation.com`

Abstract

Given a polygonal shape with holes, we investigate the topology of two types of skeletons (straight skeleton, Voronoi diagram) and the evolution of the inward offsets they induce. It is shown that both skeletons are homotopy equivalent to the shape and an $O(n \log n)$ algorithm to compute the persistent homology of the filtration of the inset polygons w.r.t. to their reversed offsetting process is given. We conclude with a brief discussion on possible applications.

1 Introduction

The straight skeleton and the Voronoi diagram of a polygonal shape capture certain topological and geometrical information. For instance, the maximum inscribed circle of the shape has its center at a vertex of of Voronoi diagram. In terms of homotopy both skeletons encode *the* topology of the shape, but their geometry is different. The different geometry manifests in different offset curves: Mitered offsets for straight skeletons and Minkowski offsets for Voronoi diagrams. The evolution of offset curves again tells something about the topology of the shape. The mathematical tool to investigate this observation is persistent homology.

Lieutier [8] showed that the medial axis of an open bounded set in $\mathbb{R}^d$ is homotopy equivalent to its medial axis by an involved proof not based on constructing a deformation retraction. Further related work concerns the homotopy of the medial axis, its stability, and its relation to the Voronoi diagram of a point set. Halperin et al. [4] investigated the outer (Minkowski) offset filtration of convex polyhedra in two and three dimensions, i.e., they generalize from (alpha filtrations of) point sets to sets of disjoint convex polyhedra and presented an $O(n \log n)$ algorithm for the persistent homology.

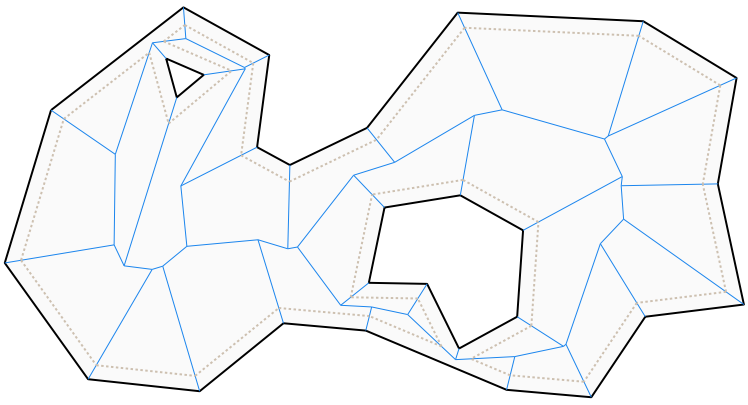

Figure 1 The straight skeleton $S(P)$ in blue of a polygon with holes, P, in black. The wavefront (a mitered offset curve) is shown as dotted lines.

34th European Workshop on Computational Geometry, Berlin, Germany, March 21–23, 2018.
This is an extended abstract of a presentation given at EuroCG'18. It has been made public for the benefit of the community and should be considered a preprint rather than a formally reviewed paper. Thus, this work is expected to appear eventually in more final form at a conference with formal proceedings and/or in a journal.

2 Topology of skeletons

Let P denote a polygon with holes in the plane, i.e., $\operatorname{bd} P$ forms a set of disjoint closed polygonal curves. The straight skeleton $S(P)$ of P is defined by a wavefront propagation process where the edges of P move inwards at unit speed. Two kind of structural changes occur to the wavefront: (i) edges may collapse and vanish and (ii) reflex vertices may hit another part of the wavefront and split it into parts.[1] The line structure that is traced out by the wavefront vertices was introduced in [1] as the straight skeleton $S(P)$ of P, see Fig. 1. We call the area swept out by one edge f of P the straight-skeleton cell $C_S(f)$ of f.

The Voronoi diagram $V(P)$ of P is defined by a nearest-neighbor cell decomposition of P by the faces of P, i.e., its vertices and edges. We follow [5] by defining the cone of influence $I(f)$ of a vertex f to be $\mathbb{R}^2$ and of an edge f to be the orthogonal strip spanned by f. Then the Voronoi cell $C_V(f)$ is defined as the set of points in $I(f)$ at least as close to f than to any other face of P. We define the Voronoi diagram $V(P)$ of P as the line structure formed by the boundaries of the Voronoi cells, restricted to P, see Fig. 2.

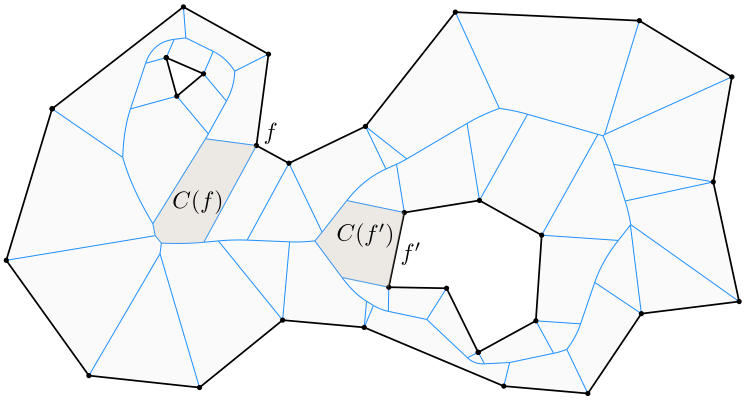

Figure 2 The Voronoi diagram $V(P)$ in blue of a polygon with holes, P, in black. Two cells $C_V(f)$ and $C_V(f')$ of the faces f and f' shaded in gray.

Two remarks on the above definition: First, for our purpose we would like to emphasize the notion of a Voronoi diagram *of a polygon* in analogy to $S(P)$ and in contrast to the typical notion of the Voronoi diagram of a collection of sites (which could form a polygon). Secondly, the two edges of $V(P)$ emanating at each reflex vertex are considered to be *topologically* disjoint, i.e., the two distinct endpoints only geometrically overlap. Furthermore, we split conic Voronoi edges at the apex, including those between two vertices of P, see [7]. This is (i) algorithmically handy, e.g., when computing offset curves, and (ii) turns out to be natural from a topological perspective.

Both, $S(P)$ and $V(P)$, capture geometrical and topological features of the underlying shape P. For instance, they form a tree for simple polygons. Moreover, for each hole that we punch into P both get a new (generator) cycle (in a group of cycles). That is, in terms of homotopy theory, they both capture *the* topology of the shape:

▶ **Theorem 2.1.** *Let P denote a polygon with holes in the plane. The following homotopy equivalences hold:*

$$P \simeq S(P) \simeq V(P).$$

[1] See [7] for a survey on straight skeletons including a taxonomy on the different wavefront events.

It suffices to show that $S(P)$ and $V(P)$ are each deformation retracts of P.

▶ **Lemma 2.2.** *$S(P)$ is a deformation retract of P.*

Proof. Consider the cell decomposition of P induced by $S(P)$. The cell $C_S(f)$ of an edge f is a topological disk [7]. Let us denote by $S(P,f) = S(P) \cap C_S(f)$ the boundary of $C_S(f)$ without f, which is a connected part of $\operatorname{bd} C_S(f)$. The topological disk $C_S(f)$ can be trivially deformation retracted to $S(P,f)$. We can even require that the deformation retraction stays constant on $S(P,f)$. This allows us to plug together the per-cell deformation retractions to a deformation retraction of $P = \bigcup_f C(f)$ to $\bigcup_f S(P,f) = S(P)$. ◀

Note that the above proof also applies to straight-skeletons of positively weighted straight skeletons. However, in the presence of negative weights Thm. 2.1 fails as $S(P)$ of a simple polygon P may have cycles as shown in [2].

▶ **Lemma 2.3.** *$V(P)$ is a deformation retract of P.*

We could use the more general result of Lieutier [8] for the medial axis, augment it with certain line segments to obtain $V(P)$ and argue that the homotopy type did not change. However, the simple proof scheme of Lem. 2.2 basically applies here, too. Moreover, Voronoi cells of circular arcs meet the above topological requirements as well [6], and hence Lem. 2.3 also applies to shapes P bounded by straight-line segments and circular arcs.

There is only a technicality at reflex vertices (for both approaches), where we remind the reader that the two emanating Voronoi edges are considered topologically disjoint. The topological space $V(P)$ could be obtained by glueing together Voronoi edges, but we do not glue at reflex vertices of P. Put in different words, let us consider P' as the Minkowski-difference[2] $P \ominus B_\epsilon$ of P by an $\epsilon > 0$, where B_ϵ denotes the o-centered ball of radius ϵ. Then $V(P') = V(P) \cap P'$, i.e., $V(P)$ is $V(P')$ with little line segments attached at the tips of $V(P')$. The shape P' is structurally the same as P, only the reflex vertices of P are replaced by tiny circular arcs of radius ϵ. We consider $V(P)$ and $V(P')$ to be topologically identical, only the tips of $V(P')$ are geometrically perturbed. In particular, we consider $V(P,f) = V(P) \cap C_V(f)$ being a topological line instead of a circle at reflex vertices.

▶ **Corollary 2.4.** *P, $S(P)$, and $V(P)$ are homologous and, by the theorem of Euler-Poincaré, have the same Euler characteristics.*

3 Persistence of offset curves

3.1 Mitered and Minkowski offsets

A skeleton and its offset curves are dual in the following sense: We can easily compute offset curves from the skeleton and, vice versa, the skeleton can be obtained from the evolution of offset curves. For the latter direction this is the original definition of straight skeletons, where the wavefront propagation is the evolution of the offset curves. The definition of Voronoi diagrams based the evolution of the offset curves is related to the so-called grassfire model.

For the former direction, the computation of mitered offset curves by means of straight skeletons resp. Minkowski offset curves by means of Voronoi diagrams are one of many

[2] For sets A, B in a vector space let $A \oplus B = \{x + y \colon x \in A, y \in B\}$ denote the Minkowski-sum and let $A \ominus B = \{x \colon \{x\} \oplus B \subseteq A\} = (A^c \oplus (-B))^c$ denote the Minkowski-difference.

applications of skeletons, e.g. in GIS (buffer zone computation) or CAD/CAM (tool-path planing in NC-machining), cf. [5, 7].

Let us denote by $Q_V(r)$ the polygon P inset by radius r according Minkowski offsetting, i.e., $Q_V(r) = P \ominus B_r$. Similarly, denote by $Q_S(r)$ the polygon P inset by radius r according to mitered offsetting. The so-called roof model projects the evolution of offset curves in three-space with the third dimension being time, see Fig. 3. We denote by $R_V(P) = \bigcup_{r \geq 0} \operatorname{bd} Q_V(r) \times \{r\}$ and likewise for $R_S(P)$. In the following we write $Q_*(r)$ resp. $R_*(P)$ when we refer to both $Q_V(r)$ and $Q_S(r)$ resp. $R_V(P)$ and $R_S(P)$. Aichholzer and Aurenhammer [1] showed the following property for $R_S(P)$, which is also true for $R_V(P)$:

▶ **Lemma 3.1.** *$R_*(P)$ does not possess local minima, except all points of $\operatorname{bd} P \times \{0\}$.*

Proof. Assume $R_*(P)$ would possess a local minimum at $q \in \operatorname{int} P$ at level $t > 0$. Then $P \setminus Q_*(t + \epsilon)$ possesses an arbitrarily small component around q for small enough $\epsilon > 0$. This basically means that offset curves pop up without being emanated from $\operatorname{bd} P$. ◀

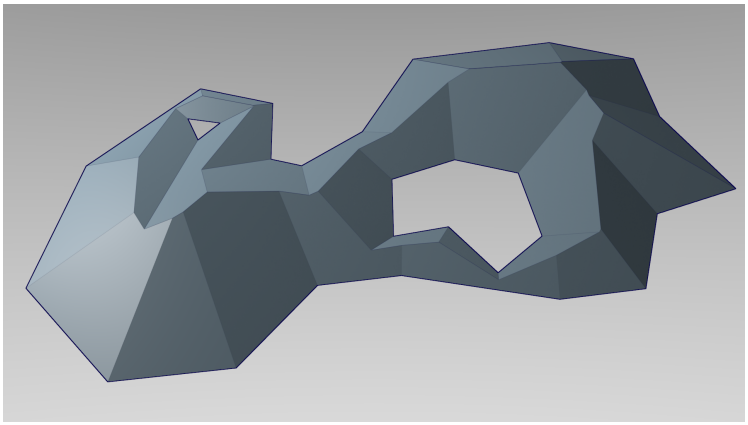

Figure 3 The straight-skeleton roof model $R_S(P)$ of P. The vertices, crests and ridges of $R_S(P)$ projected onto $\mathbb{R}^2 \times \{0\}$ give $S(P)$ again. Offset curves are lifted to isolines on $R_S(P)$.

3.2 Computing persistent homology of offset curve filtrations

Persistent homology is a mathematical framework that investigates the evolution of homology groups in a so-called filtration of topological spaces. In the following we apply this framework to a growing sequence of nested sets, where the growth is given by the offset curves with a decreasing offset radius. This gives insight into the topology of the underlying shape that goes beyond the homotopy type of P because the topological changes in the offset curves pull in geometric information from the offsetting process itself.

Let us consider r to decrease from a large enough r_0 to 0, while $Q_*(r)$ grows from the empty set to P. We ask for the persistent homology groups (over $\mathbb{Z}_2$) of this *offset filtration* of P. Using the roof model $R_*(P)$ we can apply the water shed picture [3] here: Assume the sea has level r_0 and then continuously lowers to level 0. At local maxima of $R_*(P)$ islands pop up (0-dimensional homology classes are born), at certain other levels islands merge with others (0-dimensional homology classes die) or atolls are formed (1-dimensional homology classes are born). However, from Lem. 3.1 follows this:

▶ **Lemma 3.2.** *In an offset filtration 1-dimensional homology classes never die.*

3.2.1 Direct approach on a simplicial complex

A straightforward approach to compute persistent homology could be to apply the boundary matrix algorithm [3]. To do so, we switch to the setting of a filtration on a simplicial complex. First, we consider a finite filtration: Note that the topological changes of $Q_*(r)$ only occur at levels of $R_*(P)$ where the isoline touches a roof vertex. Let us denote by $r_1 > r_2 > \cdots > r_k = 0$ the sequence of levels at which the vertices of $R_*(P)$ sit, which gives us the nested sets $Q_*(r_1) \subset \cdots \subset Q_*(r_k)$. (We may add a level $r_0 > r_1$ in order to start with the empty set $Q_*(r_0)$.) Next we construct a simplicial complex $\mathcal{C}$ that covers P by (i) adding the offset curves $\operatorname{bd} Q_*(r_1), \ldots, \operatorname{bd} Q_*(r_k)$ to the skeleton and (ii) triangulating the onion layers $Q_*(r_{i+1}) \setminus \operatorname{int} Q_*(r_i)$ for $1 \leq i \leq k-1$. Note that in step (i), we split skeleton edges at the intersection points with the offset curves and in step (ii), we only need a topological triangulation, i.e., edges do not need to be straight. Then we define a simplicial function $\mathcal{C} \to [0, \infty)$ by assigning each simplex of $\mathcal{C}$ the level of its lowest point in $R_*(P)$. We take the super-level set filtration according to this simplicial function, which corresponds to the offset filtration initially presented, i.e., it contains triangulations of all $Q_*(r_i)$ as subcomplexes.

The boundary matrix reduction runs in $O(m^3)$ time where $m \in O(kn) \subseteq O(n^2)$ is the size of $\mathcal{C}$. The construction of $\mathcal{C}$ involves the computation of k offset curves, each taking $O(n)$ time after the skeleton has been computed, and the triangulation in $O(m \log m)$ time.

3.2.2 A skeleton-based algorithm

Note that the Voronoi diagram of $Q_V(r)$ is $V(P) \cap Q_V(r)$ and similarly $S(Q_S(r)) = S(P) \cap Q_S(r)$ for straight skeletons. So $Q_V(r)$ is homotopy equivalent to $V(P) \cap Q_V(r)$ and therefore homologous. That is, instead of considering the growing sets $Q_V(r_1) \subset \cdots \subset Q_V(r_k)$ we can consider the growing subsets $Q_V(r_1) \cap V(P) \subset \cdots \subset Q_V(r_k) \cap V(P)$ of the Voronoi diagram and likewise for the straight skeleton. So it suffices to track the birth and death of components and cycles in the growing graph structure of the skeleton.

By Lem. 3.2 we can exclude the death of cycles from our considerations. So we sort the vertices of the skeleton by decreasing level in the roof model and keep adding vertex by vertex in the growing graph structure. For each new vertex v we have the following cases:

1. No neighbor of v was inserted already. Then v is a peak and a new component is born.
2. The neighbors $u_1, \ldots, u_d$ were already inserted. For every connected component that is involved with c vertices in $\{u_1, \ldots, u_d\}$ we get $c-1$ new cycles closed at v. All involved components are merged with the oldest component and then v joins this component, too.

After the skeleton of P has been computed and the vertices were sorted in $O(n \log n)$ time, where n is the number of vertices of P, one can compute the birth and death of the homology classes in $O(n\,\alpha(n))$ time by means of a union-find data structure [3]. (There are $O(n)$ find resp. union operations in case 2.) If one is interested in the homology classes itself each can be dumped in $O(n \log n)$ time by a simple graph traversal. For instance the cycle that is born at level 0.109 in Fig. 4 can be obtained by a depth-first search along one emanating edge of the vertex v at level 0.109, restricted to vertices inserted so far, until v is reached again. (The traversal stays within the component in which the cycle is closed.)

4 Conclusion

Computational topology has prominent applications in topological data analysis. We believe that also classical problems in computational geometry profit from methods of computational topology.

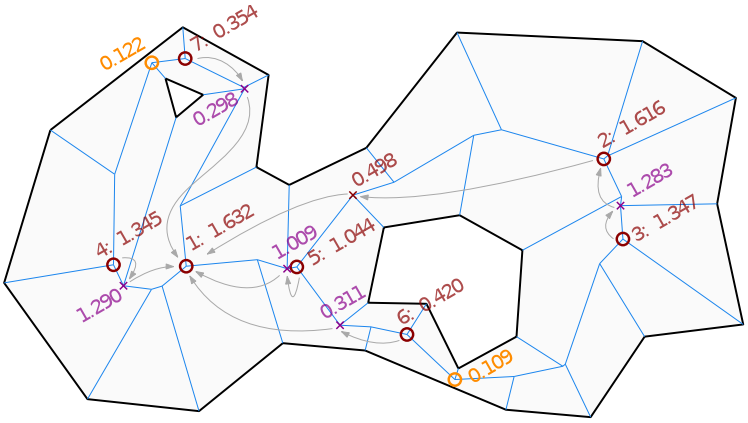

Figure 4 Birth and death of homology classes in the mitered-offset filtration by inserting vertices at given levels. Red circles are of case 1. (Peak 1 is on level 1.632.) Orange (birth of cycle) and violet (death of component) vertices are of case 2. Unlabeled vertices are trivial instances of case 2. The grey arrows tell the merge direction. Peaks in decreasing persistence: 1, 2, 6, 3, 7, 4.

Take for instance the maximum inscribed circle of P whose center is known to be a vertex of $V(P)$ with highest distance to its defining faces, i.e., the highest peak in $R_V(P)$. In other words, the maximum inscribed circle corresponds to the 0-dimensional homology class of highest persistence, where the persistence of a homology class is defined by the level difference of birth and death. We can quantify all peaks by its persistence and obtain a notion of "significance" of a locally maximum inscribed circle. This could again be useful for shape decomposition algorithms, e.g. for motion planing in NC machining. In Fig. 4 the peaks 1 and 2 have a significant persistence above 1.1, while the other peaks possess a comparable small persistence below 0.1. Those two peaks represent the "main parts" of P in this sense.

References

1 O. Aichholzer and F. Aurenhammer. Straight skeletons for general polygonal figures in the plane. In A.M. Samoilenko, editor, *Voronoi's Impact on Modern Science, Book 2*, pages 7–21. Inst. of Math. of the National Academy of Sciences of Ukraine, Kiev, Ukraine, 1998.

2 T. Biedl, M. Held, S. Huber, D. Kaaser, and P. Palfrader. Weighted straight skeletons in the plane. *Comp. Geom. Theory & Appl.*, 48(2):120–133, February 2015.

3 H. Edelsbrunner and J. Harer. *Computational Topology – An Introduction.* American Mathematical Society, 2010. ISBN 978-0-8218-4925-5.

4 D. Halperin, M. Kerber, and D. Shaharabani. The offset filtration of convex objects. In *Proc. 23rd (ESA '15)*, pages 705–716, 2015.

5 M. Held. *On the Computational Geometry of Pocket Machining*, volume 500 of *Lecture Notes Comput. Sci.* Springer-Verlag, June 1991. ISBN 3-540-54103-9.

6 M. Held and S. Huber. Topology-oriented incremental computation of Voronoi diagrams of circular arcs and straight-line segments. *Comp. Aided Design*, 41(5):327–338, May 2009.

7 S. Huber. *Computing Straight Skeletons and Motorcycle Graphs: Theory and Practice.* Shaker Verlag, April 2012. ISBN 978-3-8440-0938-5.

8 A. Lieutier. Any open bounded subset of $\mathbb{R}^n$ has the same homotopy type than its medial axis. *Comp. Aided Design*, 36(11):1029–1046, 2004.